Digital Image Correlation Method for Detecting Strain in Wood Drying Process

Haojie Chai,* Lei Cai, Tao Xu, and Yukun Ma

Stress and strain monitoring is of great significance for wood drying. Using digital image correlation (DIC), this study measured displacement and strain changes during wood drying in real time. The results showed that when wood is dried below the fiber saturation point, the difference of the radial and tangential shrinkage ratio gradually increased. An analysis of tangential and radial shrinkage ratio revealed that in the early stage of drying, the tangential and radial shrinkage ratio was relatively flat; in the middle stage of drying, the shrinkage ratio began to gradually increase; and in the later stage of drying, the tangential shrinkage ratio was approximately twice as large as that in the radial direction. Further, regarding the tangential and radial strain distribution, the radial strain distribution was more scattered than that in the tangential direction. The radial strain distribution exhibited compressive strain on both ends of the specimen, and the tensile strain was in the center. The tangential strain distribution was tensile strain on the left side of the specimen and compression strain on the right. Overall, DIC is stable and reliable, and it can be used to monitor well the stress and strain changes during wood drying.

DOI: 10.15376/biores.18.2.4143-4152

Keywords: DIC; Drying shrinkage rate; Strain distribution; Stress and strain

*Contact information: School of Artificial Intelligence, Henan Institute of Science and Technology, Xinxiang, 453003, China; *Corresponding author: nefuchj@63.com*

INTRODUCTION

Wood drying is an indispensable and important process in wood processing, and the quality of the dried wood directly affects the processing and use of wood (Ai 2016). Stress and strain during wood drying are important reference indicators for the quality of dried wood. Usually, drying stress is considered the main factor that causes defects during wood drying (Zhao and Cai 2015). Therefore, quick and accurate detection of stress and strain during wood drying is especially important.

Direct on-line detection of drying stress is difficult (Fu *et al.* 2015), and the drying stress is generally reflected by the detection of drying strain (Tu *et al.* 2004). To detect wood stress and strain during drying, scholars have proposed a variety of research methods, such as the slice, Kappa, acoustic emission, mathematical model, displacement sensor, and strain gauge methods (Cheng *et al.* 2005). These methods all indirectly speculate or calculate drying stress from strain. Therefore, these methods are difficult to operate and fail when used to perform in real-time, full-field, noncontact deformation detection for wood drying deformation. As an advanced optical deformation detection method, digital image correlation (DIC) can be used to perform real-time, full-field, and noncontact deformation detection for displacement and strain.

The DIC has gradually become an important testing method in the field of wood science. Jeong *et al*. (2010) investigated the effects of different specimen thicknesses and loading rates on using DIC to measure the Young's modulus and Poisson's ratio. The results showed that the accuracy of DIC measurements is the highest when the sample thickness was at 0.381 mm and the loading rate was at 0.254 mm/min. Gong *et al.* (2008) combined scanning electron microscopy (SEM) with DIC to obtain displacement and strain fields for different load levels. The results showed that the combination of DIC with SEM can be used to reveal the mechanism of fine and microscopic mechanical damage to wood. Peng *et al*. (2012) used three-dimensional digital image correlation (3D DIC) to measure the wood shrinkage in jack pine (*Pinus banksiana*). The results showed that the 3D DIC is a suitable method of providing localized shrinkage values, and the longitudinal, radial, and tangential shrinkages in jack pine were 0.4%, 3.3%, and 5.7%, respectively. Jeong and Park (2016) evaluated orthotropic properties of wood using DIC and achieved good results. Kuo and Wang (2019) used digital image analysis to measure the elastic properties of latewood and earlywood. To sum up, DIC technology has been widely used in the testing of wood mechanics and dry shrinkage properties, but there are few studies on the application of DIC technology in the testing of wood strain variation in the drying process.

In view of this, this study used an optical measurement system based on the DIC principle to visualize and measure the progressive deformation of wood during drying. Using samples of Mongolian pine (*Pinus sylvestris* var. *mongolica* Litv.) with dimensions of 30 mm × 30 mm × 30 mm as the research object, the changes in stress and strain during wood drying were monitored in real time. The aim of the study is to provide a theoretical basis and technical support for further research on the development of drying stress, the inhibition mechanism of the drying defect, and the formulation of suitable drying process. The main research contents are as follows: (1) DIC equipment calibration and speckle preparation; (2) influence of moisture content (MC) change on the shrinkage ratio; and (3) displacement and strain distribution analysis.

EXPERIMENTAL

Materials

A number of specimens with dimensions of 30 mm × 30 mm × 30 mm were processed from defect-free Mongolian pine. The absolute dry weighing method (Cai *et al.* 2005) was used to measure the initial MC of the specimens, and the values were in the range of 120% to 140%. Because of the high MC condition, the size of the specimen shows almost no change. To reduce the test time, the processed specimens were first placed in a chamber at a constant temperature and humidity to ensure a balanced treatment and reduce the MC of the specimens to approximately 65%. As much as possible, a uniform MC distribution of a specimen was ensured to reduce the influence of MC gradient stress.

Methods

Digital image acquisition and analysis system

As shown in Fig. 1, the VIC-3D test system was designed by American CSI Company (New York, NY, USA) based on the basic principle of digital image correlation method. The VIC-3D test system was composed of both a hardware system and a software system. The hardware system included an image acquisition card, light source, CCD (Charge Coupled Device) camera, and computer. The software system included VIC-3D

analysis software (VicSnap, American CSI Company, v.2019, New York, NY, USA) and VIC-Snap image acquisition software (VicSnap, American CSI Company, v.2019, New York, NY, USA).

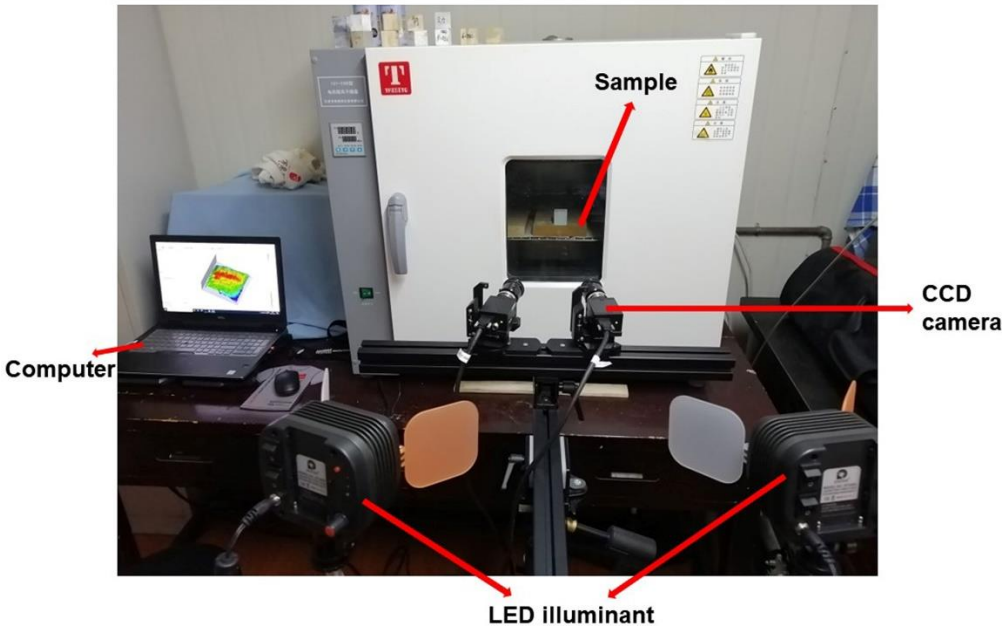

Fig. 1. VIC-3D test system

Speckle preparation

As shown in Fig. 2, speckle should be prepared on the surface of the sample before the experiment. The specimen surface should have a speckle pattern that can be recognized and contrasted. To obtain effective correlation, the speckle pattern must meet the following criteria: non-repeatability, isotropic, and high contrast. Therefore, the speckle must be random, should not be in the same direction, and must appear as dark black and bright white.

As can be seen in Fig. 3, the speckle pattern was meshed using VIC-3D analysis software and the speckle quality was analyzed. Analysis of area (AOI) was mostly blue and evenly distributed, and these observations indicated good speckle quality.

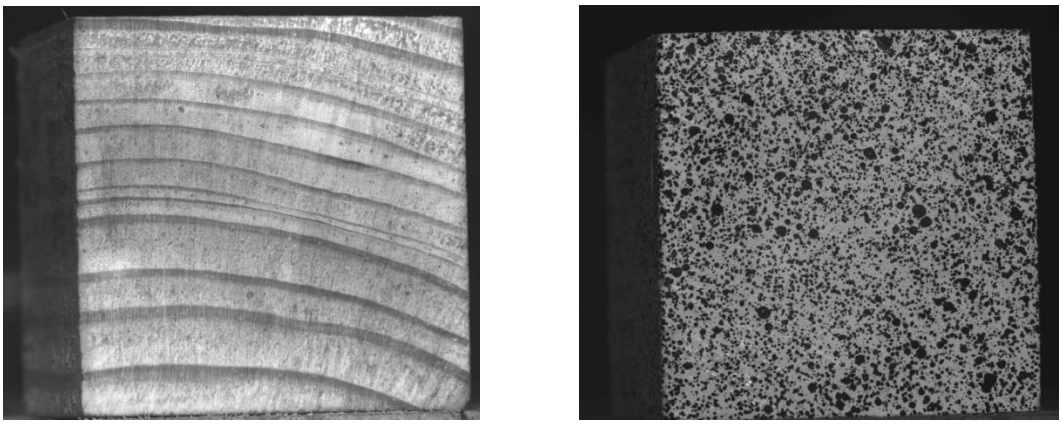

a b

Fig. 2. Speckle preparation (a: specimen and b: specklegram)

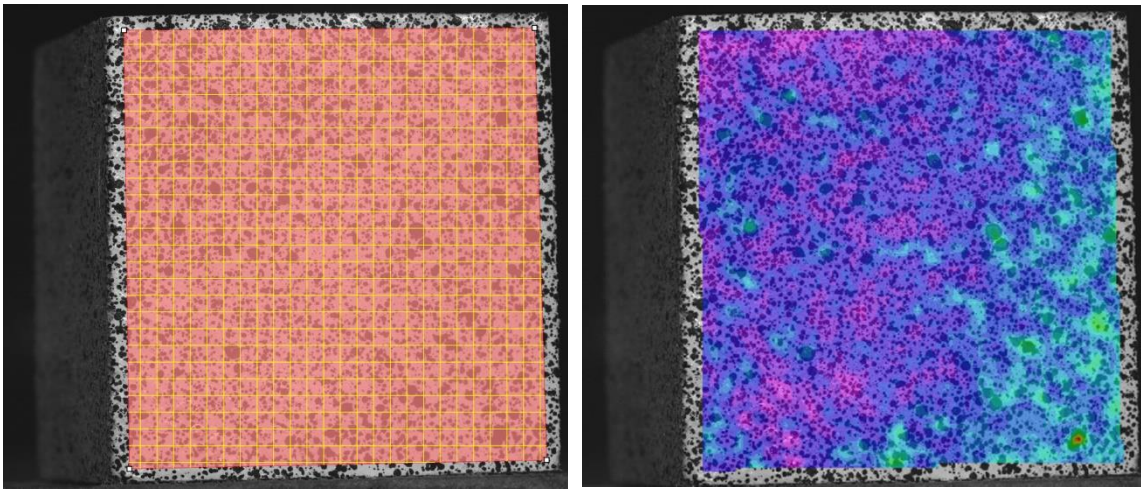

a b

Fig. 3. Analysis of area (a: mesh generation and b: speckle quality analysis)

Camera calibration

Figure 4 is a schematic diagram of the camera calibration. A suitable size calibration plate (3 mm) was selected, and the plate was placed in the vertical plane and maintained a certain flatness. Different positions were used to take photos to collect 25 to 30 calibration images. Parameter calibration was carried out *via* software analysis to test the accuracy of the calibration.

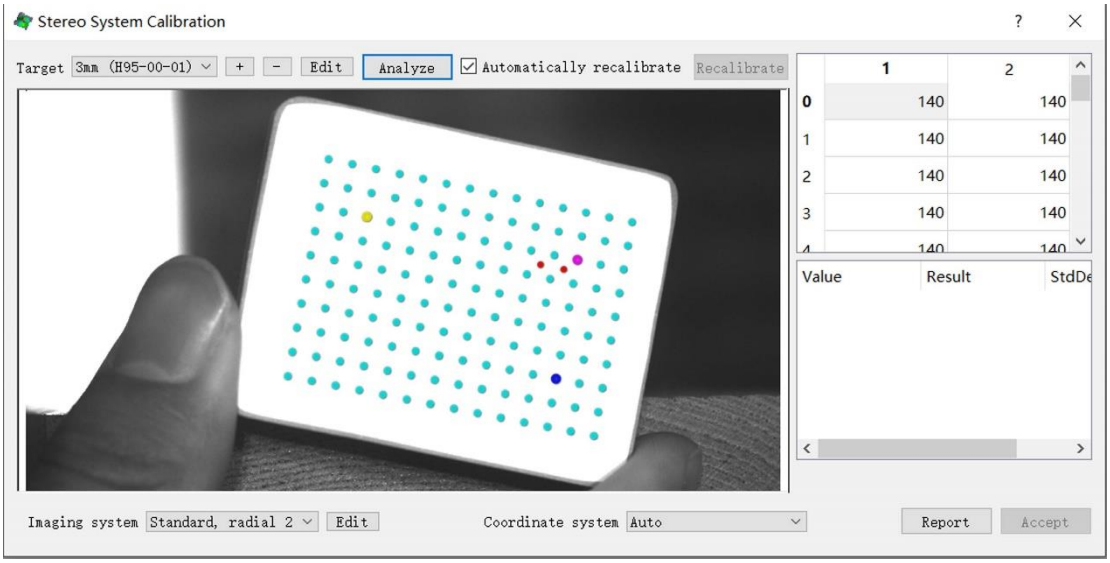

Fig. 4. Camera calibration

Detection of tangential and radial shrinkage ratio

Because wood is an anisotropic material, the tangential shrinkage ratio is about 1.2 to 2.5 times twice that of the radial component, and the longitudinal shrinkage ratio is only 1/30 to 1/40 of the radial value. Therefore, the longitudinal shrinkage ratio can be ignored, and the tangential and radial shrinkage ratios are mainly tested (Yang 2011). During wood drying, the tangential and radial shrinkage ratios are calculated according to Eqs. 1 and 2, respectively,

$$T_{SR} = (L_{Tg} - L_{Td}) / L_{Tg} \times 100\% \quad (1)$$

where T_{SR} is the tangential shrinkage ratio (%); L_{Tg} is the tangential dimension (mm) of greenwood; and L_{Td} is the tangential dimension (mm) when dried to the target MC. The radial shrinkage ratio is as follows,

$$R_{SR} = (L_{Rg} - L_{Rd}) / L_{Rg} \times 100\% \quad (2)$$

where L_{Rg} is the radial dimension (mm) of greenwood; L_{Rd} is the radial dimension (mm) when dried to the target MC.

Strain distribution detection

As can be seen in Fig. 5, the data of tangential and radial strain distributions along the central position of the specimen were extracted using VIC-3D analysis software in the drying process. The tangential and radial strain distributions data of specimens with different MC (50%, 40%, 30%, 20%, and 10%) during wood drying were obtained. Additionally, the data of displacement and strain field distributions of specimens with different MC values (50%, 45%, 40%, 35%, 30%, 25%, 20%, 15%, and 10%) were extracted using VIC-3D analysis software.

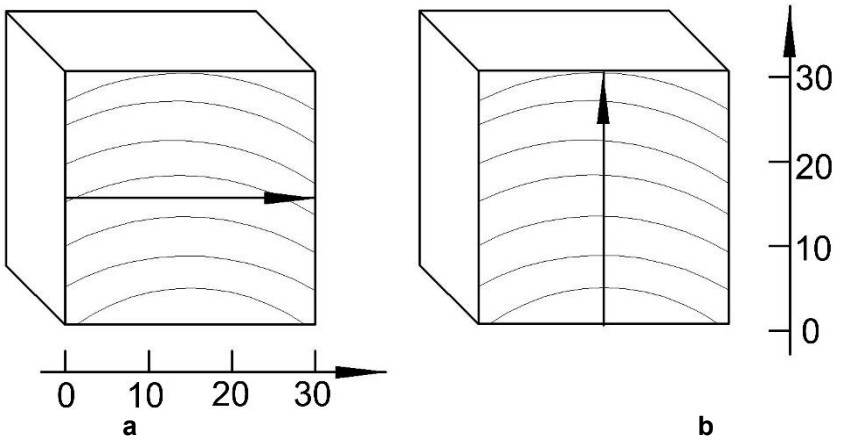

Fig. 5. Detection of tangential and radial strain distributions (a: tangential direction, and b: radial direction, unit: mm)

RESULTS AND DISCUSSION

Analysis of Strain Field Distribution

Figure 6 shows the strain field distribution diagram for specimens with different MC values. On the whole, the strain was mainly concentrated at the edges and corners, and the strain value in the center was relatively low. The tensile strain increased with a decrease in MC, and in the late drying period, it decreased slightly. The compression strain increased with MC decrease. In the early drying stage, it increased rapidly and then increased slowly, and in the late drying period, it was flat.

In the early drying period, the strain value was low and was evenly distributed. After the drying process was started, free water on the surface of the wood evaporated first. When the surface MC decreased to the fiber saturation point, dry shrinkage was produced. The surface layer was under tensile stress, and the interior was under compressive stress.

At the moment, a proper wet heat treatment for wood can effectively avoid surface checks. In the middle drying stage, changes in the strain were slight, and the internal and external stresses were temporarily in equilibrium. This is because the surface layer produced a certain degree of plasticized fixation under tensile stress.

In the late drying stage, a continuous drying process caused drying stress to accumulate continuously (Liu 2004). At that point, the MC of all parts of the wood dropped below the fiber saturation point, and the evaporation of absorbed water caused the wood to undergo dry shrinkage. An uneven distribution of MC, structural anisotropy, and growth stress generated internal stress. When part of the wood was subjected to tensile stress, the adjacent portion of the wood was subjected to compressive stress. The wood was prone to deformation and cracking at this point. A suitable second intermediate wet heat treatment was performed before cracking deformation occurred. This increased the uniformity of the wood MC distribution, restored or partially restored tensile plastic deformation of the surface layer, and released stress in advance to avoid generating drying defects.

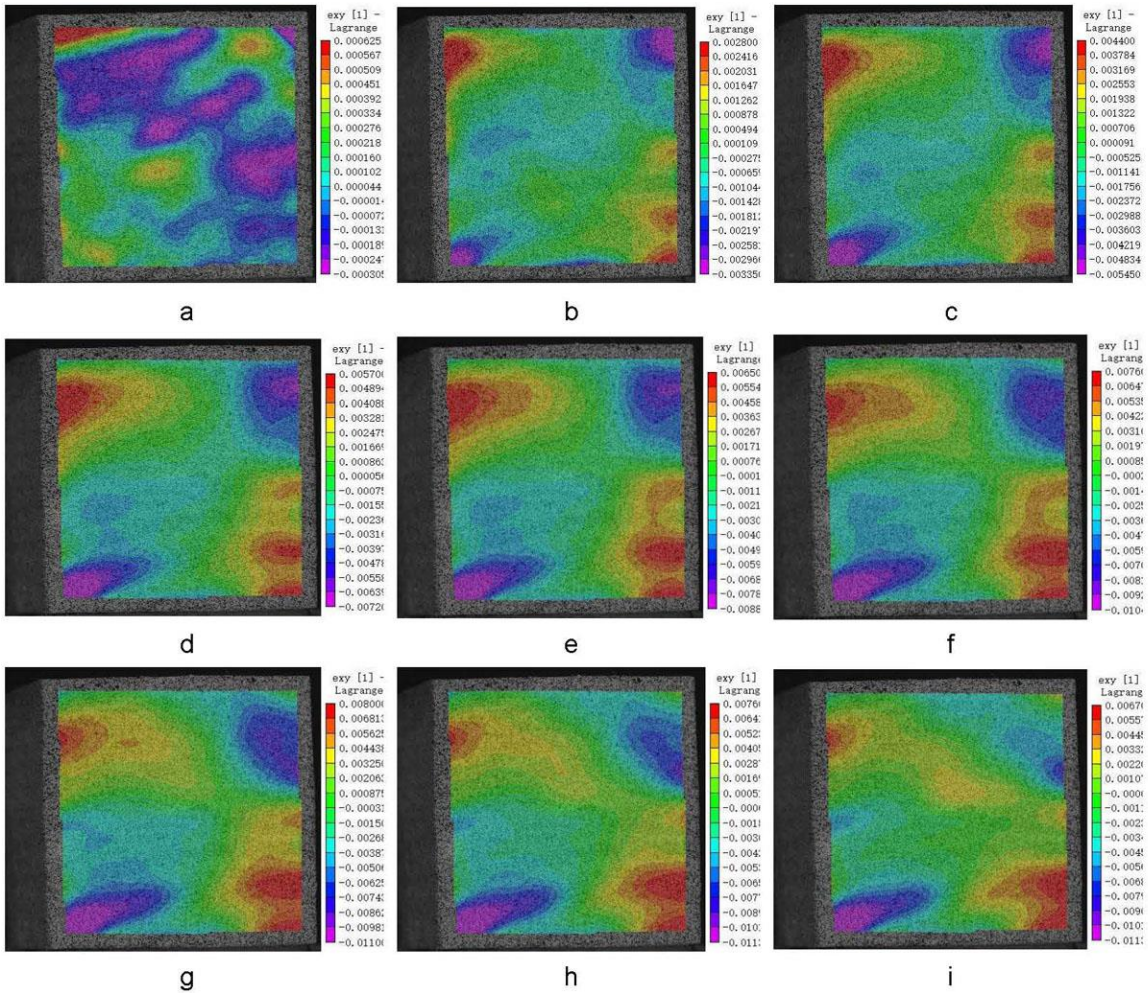

Fig. 6. Strain field distribution at different moisture content values (a through i indicate 50%, 45%, 40%, 35%, 30%, 25%, 20%, 15%, 10% of moisture content, respectively) (the darker the color, the greater the strain)

Changes in MC Before and After Pretreatment

Using the fitting equation for change in MC with respect to time, the MC of DIC specimen at each moment in the drying process was calculated. Figure 7 shows a curve diagram of changes in the tangential and radial shrinkage ratios with respect to MC. The fitting equations of the tangential and radial shrinkage ratios (T_{SR} and R_{SR}) with respect to MC were as follows:

$$T_{SR} = 2.206 \times 10^{-2} - 1.02 \times 10^{-3} MC + 1.066 \times 10^{-5} MC^2 \ (R^2 = 0.974) \quad (3)$$

$$R_{SR} = 9.37 \times 10^{-3} - 3.66 \times 10^{-4} MC + 3.57 \times 10^{-6} MC^2 \ (R^2 = 0.953) \quad (4)$$

Tangential shrinkage ratio changes

In the early stage of drying, the specimen experienced a slight thermal expansion, the tangential shrinkage ratio was negative and it was lower than the radial value. In the drying process, the shrinkage that is caused by water loss is much greater than the thermal expansion that is caused by temperature change. Additionally, the thermal expansion in the drying process is relatively small. Thus, the strain caused by thermal expansion is negligible (Liu 2004). In the middle stage of drying, the tangential shrinkage ratio increased rapidly and exceeded the radial shrinkage ratio. In the later stage of drying, the tangential shrinkage ratio was approximately twice as much as the radial, and this is basically consistent with previous studies (Lee and Jeong 2018).

Radial shrinkage ratio changes

The change of radial shrinkage ratio was relatively flat and slightly higher than the tangential direction in the early stage of drying. The shrinkage ratio was increased somewhat and lower than the tangential in the later stage of drying.

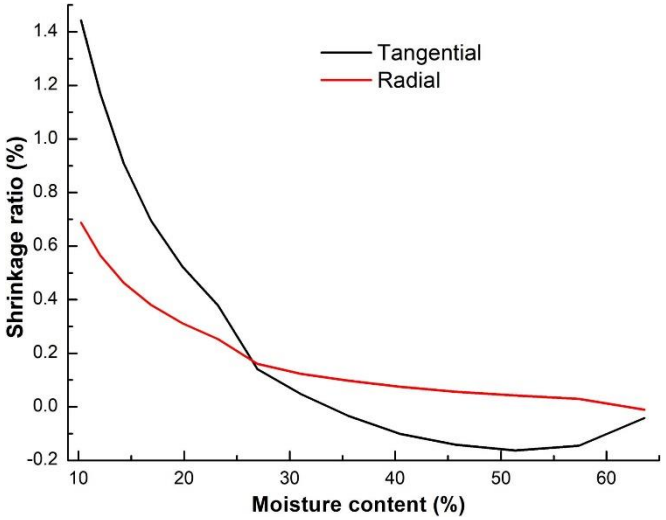

Fig. 7. Changes of tangential and radial shrinkage ratio

When MC was 40%, the specimen began to undergo dry shrinkage. There are two reasons for this. First, there is no steam in the drying process, and combined water is discharged before free water is completely discharged (Almeida *et al.* 2008). Second, in the discharge process of free water, the shape of the wood cell changes slightly, and this causes the wood size to change (Cheng 2007). Overall, above the fiber saturation point

(MC of approximately 30%), the changes in the shrinkage ratio of wood were relatively slight; below the fiber saturation point, the increase in the shrinkage ratio was more obvious. Because of wood ray inhibition for radial shrinkage and the influence of differences between earlywood and latewood, the wood showed clear dry shrinkage anisotropy.

This shows that obvious dry shrinkage is produced when the MC falls below the fiber saturation point in the wood drying process. Anisotropy of the wood structure and different shrinkage ratios in the tangential and radial directions would cause stress deformation of wood (Yang *et al.* 2016).

Tangential and Radial Strain Distribution

Figure 8 shows the tangential and radial strain distributions of specimens with different MC. Observations regarding tangential strain are as follows: In the early drying stage, the strain was small, and the strain distribution was relatively uniform. With a decrease in MC, the strain value at the end increased continuously. Tensile strain was observed on the left side, and compression strain was observed on the right side. This led to distortion and deformation of the specimen. The strain change in the center of the specimen was not obvious and was close to zero.

Observations regarding the radial strain are as follows: The strain was small and evenly distributed during the early drying stage. With a decrease in MC, the strain increased gradually, and its peak gradually moved closer to the center of the specimen. The two ends exhibited compression strain, and the center part exhibited tensile strain; this combination easily caused internal cracking during the late drying stage.

Along the tangential direction, the material distribution was relatively uniform, and the strain distribution was relatively simple. Compared to the tangential strain distribution, the strain values in the radial direction were more scattered, and the material inhomogeneity affected this. Along the radial direction, for earlywood and latewood, and for heartwood and sapwood, different positions of the material difference were large, and dry shrinkage difference was obvious.

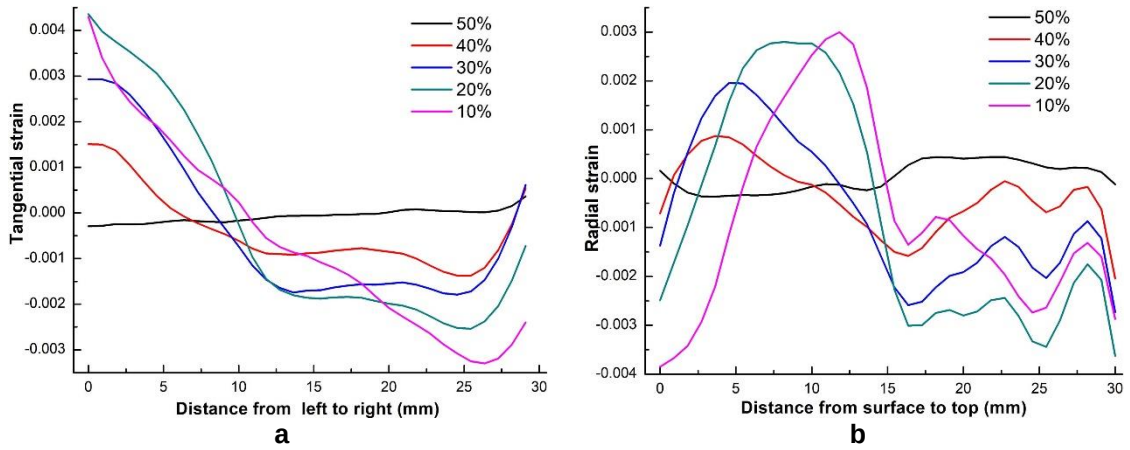

Fig. 8. Tangential and radial strain distributions (a: tangential; and b: radial)

CONCLUSIONS

1. When dried below the wood fiber saturation point, the difference of the radial and tangential shrinkage ratio gradually increased.
2. In the early drying stage, the changes in the tangential and radial shrinkage ratios were slight; in the middle drying stage, the tangential shrinkage ratio increased rapidly and was approximately twice the radial shrinkage ratio.
3. Because of differences between heartwood and sapwood, and between earlywood and latewood, the radial strain distribution was more scattered than the tangential direction. The radial strain was compressive strain at the end of a specimen and tensile strain at the center; the tangential strain distribution was tensile strain at the left of a specimen and compressive strain was found at the right.
4. In general, although the performance of different parts of wood is very different, and the online strain detection in the drying process is difficult, DIC technology can provide reliable detection capability and realize real-time online stress and strain detection in the drying process.

ACKNOWLEDGMENTS

This work was financially supported by Science and Technology Project of Henan Province (222102110205), and Key research Project of higher education institutions in Henan Province (23A520034).

REFERENCES CITED

Ai, M. Y. (2016). *Practice and Application of Wood Drying*, Chemical Industry Press, Beijing, China.

Almeida, G., Assor, C., and Perre, P. (2008). "The dynamic of shrinkage/moisture content behavior determined during the drying of micro-samples," *Drying Technol*ogy 26(9), 1118-1124. DOI: 10.1080/07373930802266108

Cai, Y. C., Chen, G. Y., and Aai, M. Y. (2005). "Discussion on improving measurement accuracy of wood moisture content by oven drying method," *Journal of Beijing Forestry University* 27, 64-67.

Cheng, W. L., and Liu, Y. X. (2005). "Characteristics of shrinkage stress of wood during drying under high temperature and high pressure steam conditions," *Journal of Beijing Forestry University* 27(2), 101-106.

Cheng, W. L. (2007). *Wood High Temperature and High Pressure Steam Drying Process Principle*, Science Press, Beijing, China.

Fu, Z. Y., Zhao, J. Y., Huan, S. Q., Sun, X. M., and Cai, Y. C. (2015). "The variation of tangential rheological properties caused by shrinkage anisotropy and moisture content gradient in white birch disks," *Holzforschung* 69(5), 573-579. DOI: 10.1515/hf-2014-0089.

Gong, C. Z., Liu, Y. Z., and Wang, Q. (2008). "Meso-scale experimental investigation and strain fields analysis of tensile tests on microtomed slices of *Picea jezoensis* var.

microsperma sample," *Scientia Silvae Sinicae* 4(3), 166-169. DOI: 10.3321/j.issn:1001-7488.2008.03.031

Jeong, G. Y., Zink-Sharp, A., and Hindman, D. P. (2010). "Applying digital image correlation to wood strands: Influence of loading rate and specimen thickness," *Holzforschung* 64(6), 729-734. DOI: 10.1515/HF.2010.110.

Jeong, G. Y., and Park, M. J. (2016). "Evaluate orthotropic properties of wood using digital image correlation," *Construction and Building Materials* 113, 864-869. DOI: 10.1016/j.conbuildmat.2016.03.129.

Kuo, T. Y., and Wang, W. C. (2019). Determination of elastic properties of latewood and earlywood by digital image analysis technique. *Wood Science and Technology* 53(3), 559-577. DOI: 10.1007/s00226-019-01096-x.

Lee, S. S., and Jeong, G. Y. (2018). "Effects of sample size on swelling and shrinkage of *Larix kaempferi* and *Cryptomeria japonica* as determined by digital caliper, image analysis, and digital image correlation (DIC). *Holzforschung* 72(6), 477-488. DOI: 10.1515/hf-2017-0120.

Liu, Y. X. (2004). *Wood Resource Materials Science*, China Forestry Press, Beijing, China.

Peng, M., Wang, Y. C., and Chui, W. C. (2012). "Measurement of wood shrinkage in jack pine using three dimensional digital image correlation (DIC)," *Holzforschung* 66(5), 639-643. DOI: 10.1515/hf-2011-0124

Tu, D. Y., Gu, L. B., Du, G. X., and Liu, B. (2004). "Study on drying strain of Masson pine sheet during drying," *Journal of Nanjing Forestry University: Natural Science Edition* 28(4), 6. DOI: 10.3969/j.issn.1000-2006.2004.04.005.

Yang, H., Cheng, W. L., and Ren, L. L. (2016). "Establishment of prediction model for mechanical properties of Larch wood modified by high-temperature and high-pressure steam," *Journal of Northeast Forestry University* 2016(004), 77-80, 85. DOI: 10.3969/j.issn.1000-5382.2016.04.017.

Yang, L. Q. (2011). *The Research of Preprocessing and Drying Characteristics of B. costata Disk*, Ph.D. Thesis, Northeast Forestry University, Harbin, China.

Zhao, J. Y., and Cai, Y. C. (2015). "Digital image correlation technology and its application to wood science," *World Forestry Research* 28(6), 53-57.

Article submitted: October 31, 2022; Peer review completed: December 10, 2022; Revised version received: March 20, 2023; Accepted: April 17, 2023; Published: April 26, 2023.
DOI: 10.15376/biores.18.2.4143-4152